Flame inhibition/suppression by water mist: Droplet size/surface area, flame structure, and flow residence time effects

H.K. Chelliah [*]

Department of Mechanical and Aerospace Engineering, University of Virginia, Charlottesville VA 22904-4746, USA

Abstract

The variation of optimal water droplet size on flame inhibition/suppression is investigated numerically by exploiting the distinct flow residence time of laminar methane–air *premixed* flames and counterflow *non-premixed* flames. For a gas inflow stream saturated with water vapor, it is shown that the relevant flow residence time of a premixed flame is governed by the droplet trajectory through the preheat region, while for a non-premixed flame, the relevant time scale is governed by the convective-diffusive layer relative to the saturated air-stream. Assuming no velocity lag between the gas and droplets at the inflow, a factor of four difference in droplet residence time is related to the predicted optimal droplet sizes of 6.5 μm for premixed flames and 20 μm for non-premixed flames. For droplets larger than the optimal size, the flame strength (defined as the square of the normalized burning velocity for premixed flames or normalized extinction strain rate for non-premixed flames) is shown to decrease linearly with increasing specific droplet surface area. As the water droplets approach the optimal size, the linear correlation stated above fails for both premixed and non-premixed flames; this failure can have major implications for the design of water-mist fire suppression systems. A comparison of present predictions and previously reported experimental data is also presented.
© 2006 The Combustion Institute. Published by Elsevier Inc. All rights reserved.

Keywords: Water-mist; Inhibition/suppression; Laminar flames; Residence time

1. Introduction

Condensed-phase agents, such as fine-water droplets or water mist, are widely used in many fire suppression/inhibition applications. Unlike gaseous-phase agents, the fine-water droplets promote fire suppression/inhibition primarily through thermal effects associated with the relatively large latent heat of vaporization. Full reali-zation of thermal effects of fine-water droplets, however, is primarily determined by the droplet size, the flame structure, and the two-phase flow field. This paper reports a detailed numerical analysis relating the above parameters to droplet residence time of two commonly used laboratory flow configurations, namely (i) freely-propagating premixed flames and (ii) non-premixed counterflow flames.

In an early investigation by Rosser et al. [1], the heating rate of condensed-phase fire suppressants (e.g. sodium bicarbonate particles) in the preheat region of a *premixed flame* was analyzed.

---

[*] Fax: +1 434 982 2037.
E-mail address: harsha@virginia.edu

Their results indicated a strong correlation between the flame inhibition effectiveness and the specific surface area of the particles, with particles below 5 μm showing no further change in their effectiveness. About two decades later, using finite-rate kinetics and large-activation energy asymptotics, Mitani [2] reinvestigated the interaction of sodium bicarbonate particles with a premixed flame structure, as well as water sprays containing alkali salts [3]. The detailed *counterflow flame* analysis in the presence of condensed-phase droplets was first considered by Continillo and Sirignano [4], where the general formulation for flame-droplet interactions was presented subjected to the self-similar approximation. While numerous analytical/numerical investigations followed [5–8], Lentati and Chelliah [9] reported a detailed numerical investigation on counterflow flame suppression with fine-water droplets as illustrated in Fig. 1. Analysis of the flame structure and critical flame extinction results have yielded quantitative information about the physical, thermal, and chemical mechanisms contributing to flame suppression [10].

In the present work, the inhibition of a one-dimensional, freely propagating *premixed flame* with fine-water droplets, as illustrated in Fig. 2, is investigated using a two-phase reacting flow model, similar to that used in non-premixed flames [9]. Although previous analyses of gaseous premixed and non-premixed flames have indicated a one-to-one correlation between the square of the burning velocity of a premixed flame, $(S_L^0)^2$, and the extinction condition of a non-premixed flame, a_{ext} [11], such correlations are shown to break down with the addition of water droplets, consis-
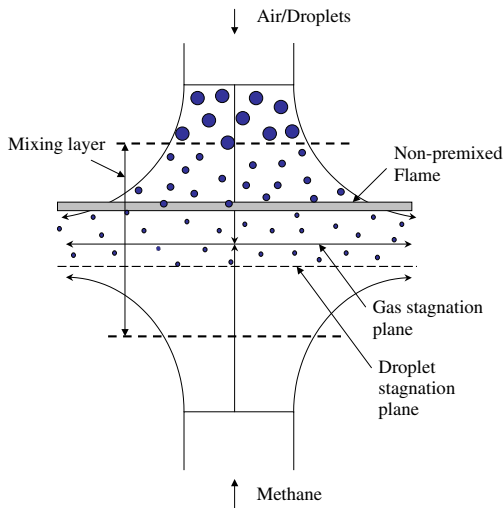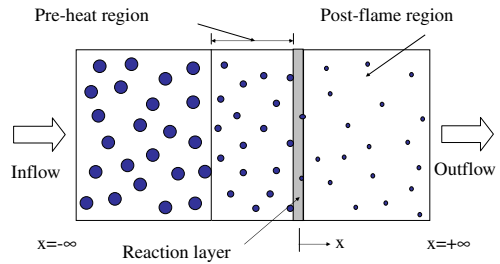

Fig. 2. Schematic of the premixed flame configuration with fine-water droplets introduced with the saturated inflow stream.

tent with the recently reported flame suppression/inhibition experiments [12]. By varying the water droplet size at the inflow boundary, it is shown that differences in flow residence times between the premixed and counterflow non-premixed flames lead to different optimal droplet sizes, the underlying reason for the breakdown in the correlation mentioned above. The differences on flame suppression effectiveness observed based on the two laboratory flow configurations imply that extension of flame suppression results to large-scale fires with complex flow fields must carefully consider the residence time and droplet size effects.

The predicted flame suppression/inhibition data are also analyzed on the basis of droplet surface area per unit mass, yielding considerable insight into the non-linear effects associated with the optimal droplet size. Specifically, the present results indicate that only droplets much larger than the optimal drop size satisfy the specific droplet surface area concepts proposed in 1960's [1], with major implications for the design of water-mist systems.

2. Formulation of two-phase premixed and non-premixed flames

A hybrid Eulerian–Lagrangian approach is used to numerically solve for the two-phase reacting flow equations describing steady, laminar premixed and non-premixed counterflow flames in the presence of fine-water droplets. In the counterflow field, under the assumption of self-similarity near the axis of symmetry, i.e. $v = v(x)$, $u = rU(x)$, $Y_i = Y_i(x)$, $T = T(x)$, where x is the axial distance, r the radial distance, v the axial velocity, u the radial velocity, $U(x)$ the x-dependent component of u, Y_i the mass fraction of species i ($i = 1, \ldots, N$) and T the temperature of the gas-phase, the Eulerian formulations for gas-phase species and energy equations are exactly the same as a one-dimensional premixed flame, and are given by

Fig. 1. Schematic of the counterflow non-premixed flame configuration with fine-water droplets introduced with the saturated air-stream.

$$\rho v \frac{dY_i}{dx} + \frac{d}{dx}(\rho Y_i V_i) = W_i \dot{\omega}_i + (\delta_{i\alpha} - Y_i)S_m \quad (1)$$

$$\rho \sum_{i=1}^{N}(v + V_i)Y_i c_{pi}\frac{dT}{dx} = \frac{d}{dx}\left(\lambda\frac{dT}{dx}\right)$$

$$- \sum_{i=1}^{N} W_i \dot{\omega}_i h_i + S_h - h_\alpha S_m. \quad (2)$$

Here, V_i, $\dot{\omega}_i$, W_i, h_i, and c_{pi} are the diffusion velocity, molar production rate, molecular weight, enthalpy, and specific heat at constant pressure of species i, respectively, while ρ and λ are the gas-mixture density and thermal conductivity, respectively. The terms on RHS, S_m and S_h are the mass and enthalpy source terms associated with evaporating droplets and $\delta_{i\alpha}$ is the Kronecker delta function, where subscript α identifies the evaporating species (in this case water). The influence of radiative transport on droplet evaporation and subsequent interaction with flames were investigated by Kee and co-workers [13,14], however, for flow residence times of the order of several msec as considered here, the radiation effects are negligible.

The main difference between the two flow fields is manifested in the mass continuity equation because of the non-uniform flow associated with the counterflow field (i.e. radial flow effect). In the presence of evaporating droplets, the mass continuity for the counterflow field is given by,

$$\frac{d}{dx}(\rho v) + 2\rho U = S_m, \quad (3)$$

while for one-dimensional premixed flames, with $U = 0$, the relevant mass continuity equation reduces to $d(\rho v)/dx = S_m$. For counterflow flames, the solution for $U(x)$ can be obtained by solving the radial momentum equation,

$$\rho v \frac{dU}{dx} + \rho U^2 = \frac{d}{dx}\left(\mu\frac{dU}{dx}\right) - J + S_U - US_m, \quad (4)$$

where μ is the coefficient of viscosity, S_U is the radial momentum source term associated with droplets, and J is the radial pressure gradient defined by $J = (1/r)(\partial p/\partial r)$. For the steady, incompressible flow considered here the leading order pressure term is set to atmospheric pressure and ρ is determined via the equation of state.

The above coupled equations must be solved subject to the appropriate boundary conditions of the two flow fields, i.e. for premixed flames,

$$x = -\infty : v = v_{-\infty}, \quad T = T_{-\infty}, \quad Y_i = Y_{i,-\infty},$$

$$x = +\infty : \frac{dT_\infty}{dx} = 0, \quad \frac{dY_{i,\infty}}{dx} = 0, \quad (5)$$

and for non-premixed flames (subscript F and O identifying the fuel and air streams),

$$x = -\frac{l}{2} : v = v_F, \quad U = U_F, \quad T = T_F, \quad Y_i = Y_{i,F},$$

$$x = +\frac{l}{2} : v = v_O, \quad U = U_O, \quad T = T_O, \quad Y_i = Y_{i,O}. \quad (6)$$

Unless otherwise mentioned, the following boundary conditions for stoichiometric premixed methane–air flame with saturated water vapor are imposed, $T_{-\infty} = 300$ K and species $Y_{CH_4,-\infty} = 0.054$, $Y_{O_2,-\infty} = 0.215$, $Y_{N_2,-\infty} = 0.708$, $Y_{H_2O,-\infty} = 0.023$. For counterflow flames with nozzle separation distance of $l = 1$ cm, the inflow conditions used are $T_F = T_O = 300$ K, $U_F = U_O = 0$ (plug flow boundary conditions), composition of fuel boundary $Y_{CH_4,F} = 1$, while that of air with saturated water vapor $Y_{O_2,O} = 0.228$, $Y_{N_2,O} = 0.749$, $Y_{H_2O,O} = 0.023$. The values of v_F and v_O are varied with momenta balanced to obtain any desired flow strain rates. The imposition of v_F and v_O for the first-order mass continuity equation yields a unique value for J, the pressure eigen value [15,16].

Once the droplet source terms S_m, S_h, and S_U, are evaluated based on the Lagrangian equations described below, finite-rate chemistry effects can be resolved accurately to analyze the thermal effects associated with the droplets.

2.1. Droplet source terms

The droplet source terms S_m, S_h, and S_U must be described based on their trajectory through the flame structure. The Lagrangian description of droplet transport is used for small droplet number density (or dilute droplet loadings) because of the concerns about the validity of continuum approximation for the condensed phase. The relevant droplet conservation equations for mass, x-momentum, and energy can be written as [9],

$$\frac{dm_d}{dt} = -\dot{m}_d, \quad (7)$$

$$\frac{d}{dt}(m_d v_d) = -\dot{m}_d v_d + 3\pi d\mu(v - v_d). \quad (8)$$

$$\frac{d}{dt}(m_d h_d) = -\dot{m}_d(h_d + L) + H, \quad (9)$$

where the subscript d refers to droplet properties. Here, d is the droplet diameter, $m_d = (\pi/6)\rho_d d^3$ the droplet mass, $\dot{m}_d$ the mass evaporation rate of the droplet, $h_d = h_d^0 + c_{p,d}(T - T_0)$ the specific enthalpy of the droplet, L the specific latent heat of vaporization, and H the heat flux to the droplet from the gas. Both $\dot{m}_d$ and H are estimated using an analytical formula derived assuming d^2-law [17], which is applicable for isolated evaporating droplets under quasi-steady evaporation conditions. In Eq. (8), the viscous drag force due to droplet motion relative to the gas-phase is based

on Stokes drag coefficient of $C_D = 24/Re_d$. This assumption is valid for droplet Reynolds number $Re_d \leqslant 1$, which is generally satisfied for cases where the initial droplet velocity is assumed to be the same as the gas velocity at the inflow boundary. Furthermore, the droplet evaporation in the cold inflow region, i.e. outside the thermal mixing layer, is avoided by saturating the gas stream with water vapor [18]. Consequently, the droplet size remains constant until the droplets enter the preheat (convective-diffusive) layer.

For counterflow flames, in addition to Eqs. (7)–(9), an equation for radial momentum of the droplets, given by

$$\frac{d}{dt}(m_d U_d) + m_d U_d^2 = -\dot{m}_d U_d + 3\pi d_d \mu (U - U_d), \quad (10)$$

coupled with the local droplet number density, n_d, must be integrated to obtain the mass source terms S_m, S_h, and S_U that appear in Eqs. (1)–(4). For counterflow flames, n_d will vary with axial location and its variation can be obtained by integrating the following equation for droplet flux fraction, $\mathcal{F}(t)$ [9]

$$\frac{d\mathcal{F}}{dt} + 2\mathcal{F}U_d = 0. \quad (11)$$

Here, $\mathcal{F} = 1$ at the droplet inflow boundary, but $\mathcal{F}$ will decrease rapidly as the droplets approach the stagnation plane because of the flow straining effect. In one-dimensional premixed flames, assuming negligible droplet coalescence or break-up, n_d remains constant across flame structure (i.e. $\mathcal{F} = 1$ everywhere).

To outline the approach used to evaluate the droplet source terms, let ϕ denote the right-hand side terms of Eqs. (7)–(10) (i.e. $-\dot{m}_d$, $-\dot{m}_d v_d + 3\pi d\mu(v - v_d)$, $-\dot{m}_d(h_d + L) + H$, and $-\dot{m}_d U_d + 3\pi d\bar{\mu}(U - U_d)$). In terms of ϕ, the droplet source terms in Eqs. (1)–(4) contributing to an arbitrary grid point j with a grid size of dx_j, can be written as

$$S_{\phi j} = -(1/dx_j) n_{d_0} v_{d_0} \sum_{k=1}^{K_j} \int_{t_k}^{t_k + dt_k} \mathcal{F}(t)\phi \, dt, \quad (12)$$

where at each cell j the integration of Lagrangian equations are performed in K_j time steps with step size of dt_k. Here n_{d0} is the droplet number density at the inflow boundary and v_{d0} is the velocity of droplets, assumed to be same as the gas-velocity. For one-dimensional premixed flames, Eq. (12) is still applicable with the constraint that U and U_d are identically zero.

2.2. Numerical method

In the absence of droplet source terms, numerical integration of Eqs. (1)–(4) describing non-pre-mixed and premixed flame propagation using a modified-Newton approach is well established [16,19]. In the presence of evaporating water droplets, a similar modified-Newton approach coupled with the source terms arising from the integrated Lagrangian equations of droplet motion has been previously adopted by [6,9,13]. In particular, the Lagrangian equations describing the droplet motion are integrated via a mixed explicit–implicit scheme, as described in [9]. The approach selected is based on numerical stability in the limit the time-step size $\delta t_n \to 0$ in Eq. 12. Provided the droplet does not travel more than a fraction of the local grid size, the source terms determined by integration of Lagrangian equations yield stable consistent results.

The thermochemical and transport properties in the conservation equations are calculated using the Sandia Chemkin and transport libraries [20,21]. The detailed chemical reaction model for methane–air system used consists of 17 species in 39 elementary reactions [22].

3. Results and discussion

Based on phenomenological concepts and more rigorous large-activation energy asymptotic solution approaches, it can be shown that the burning velocity of a premixed flame is proportional to the square-root of the chemical reaction rate. The overall burning rate, however, can be inhibited by several mechanisms, namely chemical mechanisms via scavenging of radical species, thermal mechanisms via decrease of flame temperature, and physical mechanisms via dilution or flow field modifications. In general, flame inhibitors may include one or several of the above mechanisms, however, the focus here is to understand the dominant thermal suppression mechanism of fine-water droplets.

In experiments, the fuel–air mixture is expected to be saturated with water vapor if water droplets are introduced sufficiently upstream of the premixed flame [12,18]. For a typical inflow pressure and temperature of 1 atm and 300 K, the saturation mass fraction of water vapor is 0.023 (or 0.035 in mole fraction). The resulting dilution or displacement of the fuel-air mixture by water vapor can reduce the burning velocity of the premixed flame. For example, the predicted burning velocity of a dry stoichiometric, methane–air flame of $S_L^0 = 40.8$ cm s^{-1} reduces to $S_{L,vap} = 34.9$ cm s^{-1} with addition of saturated water vapor, about 14% reduction. Since the focus here is on condensed phase mass addition, the flame burning velocity results with addition of fine-water droplets are normalized by $S_{L,vap}$. An important implication of imposing saturated water vapor condition is that the droplets entering the computational domain (i.e. $x = -\infty$) do not

evaporate until they reach the preheat (convective-diffusive) region of the premixed flame, as illustrated in Fig. 2. Therefore, the droplet residence time in the cold upstream region of the flame structure is of no consequence in terms of mass evaporation.

3.1. Droplet transport and source terms

When a significant mass fraction of water droplets is introduced, the flame burning velocity decreases significantly with changes in the flame structure. For the purpose of analyzing droplet history and dynamics, (e.g. droplet size, temperature, and velocity) and the distribution of source terms contributing to the flame inhibition, the coupling source terms are initially turned "off" in the gas-phase equations, i.e. $S_m = S_U = S_h \equiv 0$. Under such uncoupled conditions with the flame structure unaffected, Fig. 3 shows the variation of normalized droplet size (d/d_0 where d_0 is the initial droplet size at the inflow boundary) for several initial monodispersed droplet sizes of 10, 20, and 30 μm. It is seen that the small droplets evaporate rapidly upon entering the preheat region of the premixed flame, while the larger droplets continue to evaporate downstream of the flame, in the post-flame region. The observed variation in evaporation rate with decreasing droplet size can be directly related to the increased surface area to volume ratio of the droplet. For dilute droplet loading and low shear flows, it is reasonable to assume negligible droplet coalescence or break-up, hence the droplet distribution will remain monodispersed at any given cross-section while their size will decrease across the flame structure.

The gas velocity increases rapidly (because of the gas expansion) across the steady premixed flame structure. Consequently, the motion of relatively large droplets, introduced with the same initial velocity as the gas, may show a velocity lag

Fig. 4. Comparison of the gas and droplet velocity across the premixed flame structure, for different initial droplet sizes. Also shown is the gas-phase temperature vs. distance.

compared to the gas, as seen in Fig. 4. The droplet response to such sudden velocity variation can be characterized by Stokes number, defined as $St = t_d/t_f$, where t_d is the droplet response time given by $t_d = \rho_d d_d^2/(18\mu)$ and t_f is the flow response time given by $t_f \approx \delta/S_L$. Here δ is the characteristic flame thickness, essentially the thickness of the preheat zone. For droplets of 10 μm, the estimated values for $St = 0.04$ and for 30 μm it is $St = 0.34$. As seen from Fig. 4, with increasing St, the velocity lag between the droplets and the gas increases. Besides the velocity lag effect, the droplet temperature (T_d and uniform inside the droplet) may lag from the thermal equilibrium temperature ($T_{d,equil}$) as the droplet size increases, i.e. when the heat flux to the droplet is equal to the latent heat of evaporation. Figure 5 shows a comparison of the predicted droplet temperature with the equilibrium droplet temperature indicating that small droplets follow $T_{d,equil}$ closely while the larger droplets lag $T_{d,equil}$ slightly (note: $T_{d,10\mu m} \equiv T_{d,equil}$). Because of the relatively
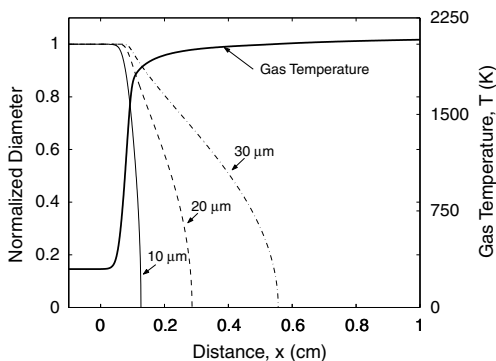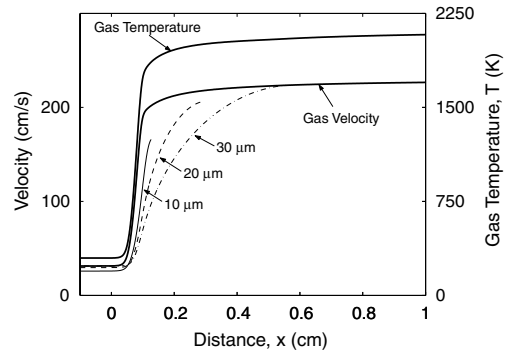

Fig. 3. Variation of normalized droplet diameter across the premixed flame structure, for different initial droplet sizes. Also shown is the gas-phase temperature vs. distance.
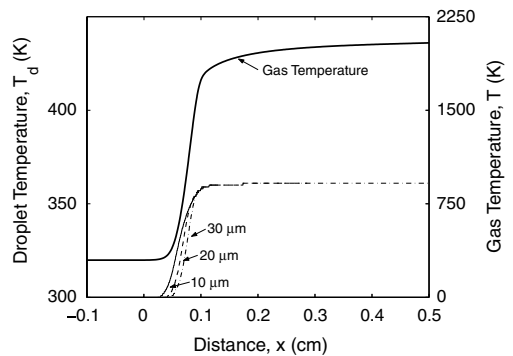

Fig. 5. Comparison of gas and droplet equilibrium temperature (T_{equil}) across the premixed flame structure, for different initial drop sizes.

low evaporation temperature of water, this subtle difference has no significant effect on the predicted results.

With gas-droplet coupling turned "off," Figs. 6 and 7 show the mass source term (S_m) and the enthalpy source term ($S_h - h_\alpha S_m$), respectively, for selected droplet sizes. The magnitude of the source terms depends on the droplet loading, which can be characterized by the initial droplet mass fraction (Y_0) defined as $Y_0 = m_{d0}n_{d0}v_{d0}/(m_{d0}n_{d0}v_{d0} + \rho_{-\infty}v_{-\infty})$, where m_{d0} is the initial mass of the droplet. For $Y_0 = 0.02$, Fig. 6 shows that 10 μm droplets have a rapid mass evaporation rate at the flame front, hence the maximum thermal cooling effect near the peak heat release region associated with the enthalpy source terms as shown in Fig. 7, while 30 μm droplets show a broad evaporation region with significant mass and energy transfer in the post-flame region. The enthalpy source terms in the post-flame region

seen for large droplets can affect the flame via modification of the downstream boundary condition due to heat loss, however with a secondary impact on the flame inhibition.

3.2. Premixed flame inhibition and comparisons with non-premixed flames

When the droplet interaction with homogeneous kinetics is turned "on" (i.e. $S_m \neq 0$, etc.), a significant inhibition of the flame burning velocity is expected, depending on the droplet loading and size. For the purpose of comparison of premixed flame inhibition results with counterflow non-premixed flame extinction results, the square of the normalized burning velocity of a premixed flame is defined here as the flame strength, $\mathcal{S} = (S_L/S_{L,vap})$.[2] Figure 8 shows the variation of the predicted flame strength vs. droplet mass fraction (Y_0) for several initial droplet sizes. The previously reported experimental data [12] with a median droplet size of 13 μm is also shown in Fig. 8 indicating a reasonable agreement with the present predictions. The existence of an optimal droplet size can be clearly demonstrated by plotting $\mathcal{S}$ vs. d_0 as shown in Fig. 9, with Y_0 as a parameter. For $Y_0 = 0.03$ and a range of droplet sizes considered, flame strength $\mathcal{S}$ is seen to asymptote as d_0 approaches 6.5 μm. Our previous numerical work [9,10], however, has shown that a different optimal droplet size ($\sim$15–20 μm) exists for counterflow non-premixed flames, as shown in Fig. 10. The distinct optimal droplet size for the two flame configurations considered can be explained by considering the flow residence times of the two flames, as discussed below.

For droplet water mass fraction $Y_0 = 0.01$ and optimal drop size of 6.5 μm (see Fig. 9), the premixed burning velocity is 29 cm s^{-1}. Based on the droplet trajectory through the preheat layer of this flame, the integrated droplet residence time
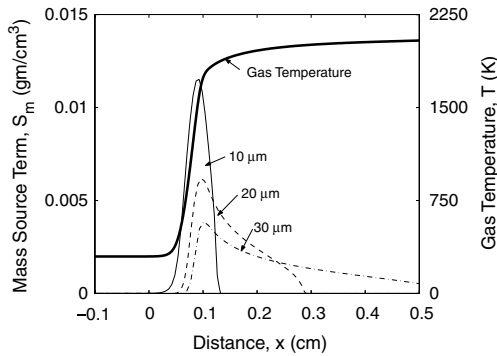

Fig. 6. The mass source term (S_m) across the premixed flame structure, for different initial droplet sizes and $Y_0 = 0.02$. Also shown is the gas-phase temperature profile.
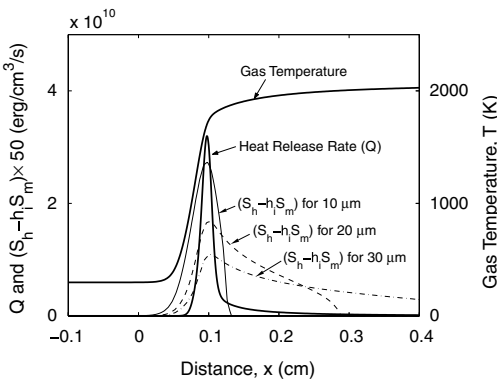

Fig. 7. The enthalpy source term ($S_h - h_i S_m$) across the premixed flame structure, for different initial droplet sizes and $Y_0 = 0.02$. Also shown is the gas-phase temperature and heat release rate profiles.
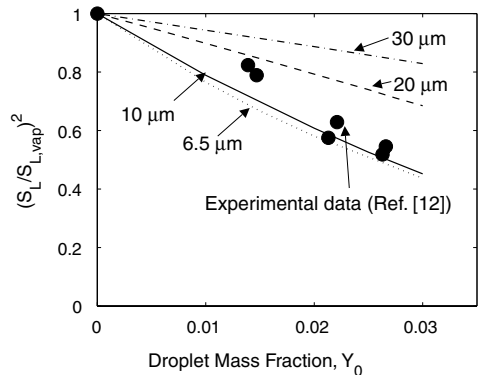

Fig. 8. Variation of the flame strength of a premixed flame vs. droplet mass fraction, for different initial drop sizes.
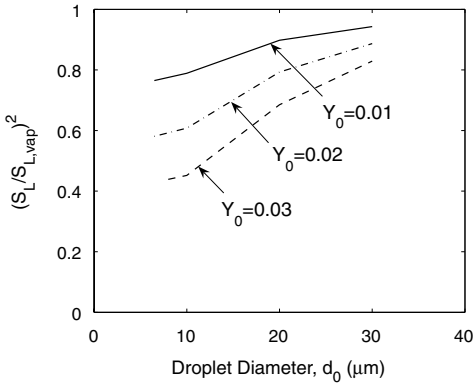
Fig. 9. Variation of the flame strength of a premixed flame vs. droplet diameter, for selected water mass fractions Y_0.
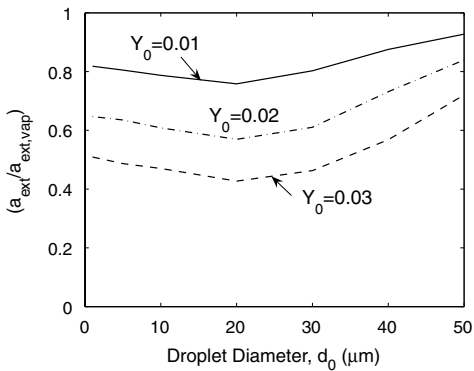

Fig. 10. Variation of the flame strength of a non-premixed flame vs. droplet diameter, for selected water mass fractions Y_0.

is 4.1 ms. In contrast, for a non-premixed flame with the same $Y_0 = 0.01$ and drop size of 20 μm, the flame extinction strain rate is 287 s^{-1}. The corresponding integrated residence time of a droplet entering the convective-diffusive layer on the air-side of the non-premixed flame is 16.2 ms. Besides the subtle difference in temperature profile and water vapor pressure, this factor of 4 difference in the residence time is the primary reason for variation of optimal droplet size between the two laboratory flames considered. While such variation in residence time on the effectiveness of droplet/particle size has been previously understood qualitatively [23], this is the first time quantitative optimal drop size data has been presented based on two commonly used laboratory flames.

3.3. Droplet surface area effect

In early studies on condensed-phase fire suppressants, a significant emphasis was placed on

the specific particle surface area [1]. Further analysis of the present numerical results in the context of such surface area concepts highlights interesting limitations of this important hypothesis.

Assuming that the fine-water droplets always remain spherical, the surface area of monodispersed droplets per unit mass is proportional to $Y_0/d_0 \equiv \mathcal{A}_s$. An identical value for the specific surface area parameter $\mathcal{A}_s$ can be realized by various combinations of inflow droplet mass loading Y_0 and droplet size d_0. Following this definition of $\mathcal{A}_s$, all the flame strength results shown in Fig. 9 for *premixed* flames are presented in Fig. 11 as a function of $\mathcal{A}_s$. Several intriguing conclusions can be drawn from Fig. 11, namely for droplets greater than 6.5 μm, the premixed flame strength $(S_L/S_L^0)^2$ decreases linearly with increasing $\mathcal{A}_s$. But, for optimal droplet size of 6.5 μm or smaller, a significant departure from the linear behavior is observed.

Furthermore, based on the flame extinction data shown on Fig. 10, a similar plot for *non-premixed* flame strength $a_{\text{ext}}/a_{\text{ext,vap}}$ as a function of $\mathcal{A}_s$ can be constructed as shown in Fig. 12. Once again, for droplets greater than the optimal size of 20 μm, the flame strength varies linearly with $\mathcal{A}_s$. The optimal droplets or smaller (i.e. $d_0 \leqslant 20$ μm) clearly deviate from this linear trend.

The new results presented in Figs. 11 and 12 can have a significant impact on design of optimal fine-water (or mist) fire-suppression systems. Specifically, if the water mist used is well above the optimal droplet size based on the characteristic residence time of the relevant flame structure (i.e. premixed or non-premixed, laminar or turbulent, etc.), then simple surface area per unit mass analysis is sufficient to determine the water-mist loading, or the size. On the other hand, if the water droplet employed is of the optimal size or smaller, then a simple linear correlation between
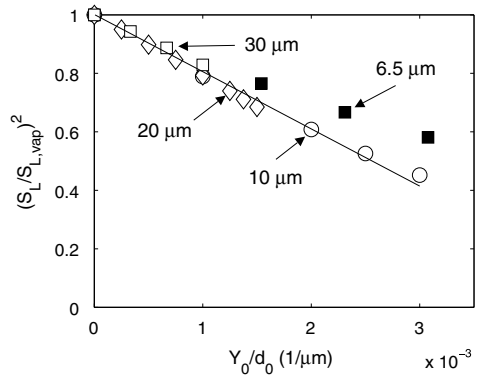

Fig. 11. Variation of the flame strength of a premixed flame vs. droplet surface area parameter ($\mathcal{A}_s = Y_0/d_0$). The line is a linear fit through predicted data for $d_0 \geqslant 10$ μm.
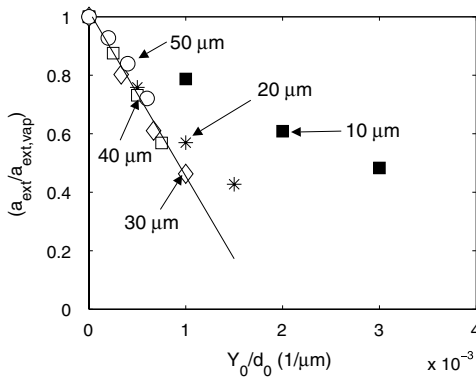
Fig. 12. Variation of the flame strength of a non-premixed flame vs. droplet surface area parameter ($\mathcal{A}_s = Y_0/d_0$). The line is a linear fit through predicted data for $d_0 \geqslant 30 \ \mu m$.

flame strength and surface area parameter shown in Figs. 11 and 12 will yield an inaccurate estimate for Y_0. Consequently, any future design of water-mist systems with optimal droplet size distributions must carefully consider the nonlinear interactions between thermal and finite-rate effects to determine the true mass loading.

4. Conclusions

The purpose of this paper is to present quantitative information about the coupling between optimal water droplet (or mist) size and the flow residence time in suppression/inhibition of gaseous flames. For a case where the water droplets were introduced with the same velocity as the gas velocity, by considering two distinct flame structures with a factor of four difference in flow residence times, it was shown that the optimal monodispersed water droplet size can vary from 20 to 6.5 μm.

Another important finding of the present work is that the commonly assumed hypothesis about droplet surface area per unit mass is only applicable for droplet sizes greater than the optimal drop size that inhibits or extinguishes the flame. By considering both premixed and non-premixed flames with distinct optimal drop sizes, it has been conclusively shown that as the optimal drop size is approached, the non-linear coupling between thermal effects and finite-rate chemistry leads to the break down of the linear correlation between flame strength and surface area parameter. This new finding can have a significant impact on design of optimal water mist systems where the water supply is limited, for example water-mist fire suppression systems in space applications.

References

[1] W.A. Rosser, S.H. Inami, H. Wise, *Combust. Flame* 7 (1963) 107–119.
[2] T. Mitani, *Combust. Flame* 43 (1981) 243–253.
[3] T. Mitani, T. Niioka, *Combust. Flame* 55 (1984) 13–21.
[4] G. Continillo, W.A. Sirignano, *Combust. Flame* 81 (1990) 325–340.
[5] F. Lacas, N. Darabiha, P. Versaevel, J.C. Rolon, S. Candel, *Proc. Combust. Inst.* 24 (1992) 1523–1529.
[6] N.-H. Chen, B. Rogg, K.N.C. Bray, *Proc. Combust. Inst.* 24 (1992) 1513–1521.
[7] K. Prasad, C. Li, K. Kailasanath, C. Ndubizu, R. Ananth, P. Tatem, *Combust. Sci. Technol.* 132 (1998) 325–364.
[8] G.O. Thomas, *Combust. Flame* 130 (2002) 147–160.
[9] A.M. Lentati, H.K. Chelliah, *Combust. Flame* 115 (1998) 158–179.
[10] A.M. Lentati, H.K. Chelliah, *Proc. Combust. Inst.* 27 (1998) 2839–2846.
[11] N. Peters, *Combust. Sci. Technol.* 30 (1983) 1–17.
[12] H.K. Chelliah, A.K. Lazzarini, P.C. Wanigarathne, G.T. Linteris, *Proc. Combust. Inst.* 29 (2002) 369–376.
[13] W. Yang, R.E. Kee, *Combust. Flame* 130 (2002) 322–335.
[14] S.P. Fuss, E.F. Chen, W. Yang, R.E. Kee, B.A. Williams, J.W. Fleming, *Proc. Combust. Inst.* 29 (2002) 361–368.
[15] R.J. Kee, J.A. Miller, G.H. Evans, G. Dixon-Lewis, *Proc. Combust. Inst.* 23 (1990) 1479–1493.
[16] M.D. Smooke, J. Crump, K. Seshadri, V. Giovangigli, *Proc. Combust. Inst.* 23 (1990) 463–470.
[17] C.K. Law, *Prog. Energy Combust. Sci.* 8 (1982) 171–201.
[18] A.M. Lazzarini, R.H. Krauss, H.K. Chelliah, G.T. Linteris, *Proc. Combust. Inst.* 28 (2000) 2939–2945.
[19] R.J. Kee, J.F. Grcar, M.D. Smooke, J.A. Miller, Sandia Report SAND85-8240, 1985.
[20] R.J. Kee, G. Dixon-Lewis, J. Warnatz, M.E. Coltrin, J.A. Miller, Sandia Report SAND86-8246, July 1992.
[21] R.J. Kee, F.M. Rupley, J.A. Miller, Sandia Report SAND89-8009B, January 1993.
[22] N. Peters, B. Rogg (Eds.), *Reduced Kinetic Mechanisms for Applications in Combustion Systems, Lecture Notes in Physics*, Vol. m15, Springer Verlag, Berlin–Heidelberg, 1993.
[23] G. Grant, J. Brenton, D. Drysdale, *Prog. Energy Combust. Sci.* 26 (2000) 79–130.

Comments

Yuji Nakamura, Hokkaido University, Japan. Could you comment on the possible reason for breaking the classical surface area correlation in small mist? Is this because the mist is not in a liquid phase (rather gas phase) in the flame zone?

In the experiment, it could be possible that droplets would gather together (increase in diameter) before moving into the flame sheet. Is there any chance this may cause the discrepancy between your single diameter prediction?

Reply. Effectiveness of large droplets (>optimal size) is clearly governed by the thermal diffusion across the boundary layer, hence the observed linear correlation with specific surface area. As correctly pointed out, for optimal or smaller droplets, the effectiveness is not directly related to the surface area, but is a function of the location where the maximum cooling due to latent heat of vaporization occurs, i.e., reaction layer or pre-heat layer.

The maximum condensed water mass fraction considered is $Y_0 = 0.03$ and corresponding ratio of droplet–droplet separation distance to droplet diameter is greater than 20. Under these conditions, the probability of droplet coalescence is negligible hence the droplet size distribution is expected to remain monodispersed. It should be pointed out that premixed flame inhibition predictions shown in Fig. 8 indicate reasonable agreement with experiments; however, I have no explanation for the differences observed in non-premixed flame suppression comparisons.

●

Michael Delichatsios, University of Ulster, UK. Can you comment on the effect of flame radiation (dominant in fires) on the determination of any "optimal" size?

Reply. In the present laboratory flames with short flow residence times, the radiation effects are not important. However, in large-scale fires, the radiation field can clearly influence the optimal droplet size. Furthermore, the departure of the droplet inflow velocity from the inflow gas velocity (assumed to be identical here) can also affect the optimal droplet size.

●

James W. Fleming, Naval Research Laboratory, USA. Was gravity included in your counter-flow calculations? An estimation of the location of the aerosol oscillatory plan suggests that drops might reside longer in the flame region if delivered with the air from the lower tube. Could this be a reason for the disagreement you report?

Reply. In numerical simulation of counterflow flames under high-strain rates, the gravity effects are not important. However, in experiments with large cross-sectional feed tubes where the gas-velocity approaches the settling velocity of droplets, a shift in the droplet size distribution may be experienced depending on whether droplets are introduced from the top or the bottom nozzle. We have accounted for such shift in droplet size distribution at the nozzle exit, so it is unlikely that gravity is the cause for the observed differences in counterflow flames.